Appl. Math. Mech. -Engl. Ed., **41**(4), 637–654 (2020)

Applied Mathematics and Mechanics (English Edition)

https://doi.org/10.1007/s10483-020-2599-7

Effects of magnetic Reynolds number on swimming of gyrotactic microorganisms between rotating circular plates filled with nanofluids*

Lijun ZHANG[1], M. B. ARAIN[1,2], M. M. BHATTI[1,†], A. ZEESHAN[2], H. HAL-SULAMI[3]

1. College of Mathematics and Systems Science, Shandong University of Science and Technology, Qingdao 266590, Shandong Province, China;
2. Department of Mathematics and Statistics, International Islamic University, Islamabad 44000, Pakistan;
3. Nonlinear Analysis and Applied Mathematics (NAAM)-Research Group, Department of Mathematics, Faculty of Science, King Abdulaziz University, Jaddeh 21589, Saudi Arabia

(Received Jan. 11, 2020 / Revised Feb. 4, 2020)

Abstract The three-dimensional (3D) nanofluid flow among the rotating circular plates filled with nanoparticles and gyrotactic microorganisms is studied. A generalized form of the magnetic Reynolds number is used for the mathematical modeling of the ferro-nanofluid flow. The torque effects on the lower and upper plates are calculated. A differential transform scheme with the Padé approximation is used to solve the coupled highly nonlinear ordinary differential equations. The results show that the squeeze Reynolds number significantly suppresses the temperature, microorganism, and nanoparticle concentration distribution, and agree well with those obtained by the numerical method.

Key words swimming of microorganism, generalized magnetic Reynolds number, nanofluid, differential transform solution, circular rotating plate

Chinese Library Classification O361
2010 Mathematics Subject Classification 76W05, 76U05, 76T10, 65Z05

Nomenclature

H_θ,	axial components;		plate (K);
H_z,	azimuthal components;	T_u,	constant temperature of the upper plate (K);
μ_1,	magnetic permeability inside the plate;	C_l,	concentration at the lower plate;
μ_2,	magnetic permeability outside the plate;	C_u,	concentration at the upper plate;
μ_f,	free space permeability ($\mathrm{N\cdot A^{-2}}$);	p,	pressure (Pa);
$B(r,\theta,z)$,	induced magnetic field;	ρ,	fluid density ($\mathrm{kg\cdot m^{-3}}$);
T_l,	constant temperature of the lower	μ,	fluid viscosity ($\mathrm{N\cdot s\cdot m^{-2}}$);

* Citation: ZHANG, L. J., ARAIN, M. B., BHATTI, M. M., ZEESHAN, A., and HAL-SULAMI, H. Effects of magnetic Reynolds number on swimming of gyrotactic microorganisms between rotating circular plates filled with nanofluids. *Applied Mathematics and Mechanics* (*English Edition*), **41**(4), 637–654 (2020) https://doi.org/10.1007/s10483-020-2599-7

† Corresponding author, E-mail: mmbhatti@sdust.edu.cn

δ, electrical conductivity ($S \cdot m^{-1}$);
T, temperature (K);
C, concentration;
T_m, mean fluid temperature (K);
c_p, specific heat ($J \cdot kg^{-1} \cdot K^{-1}$);
D_B, Brownian diffusivity;
D_T, thermophoretic diffusion coefficient;
j, microorganism flux;
R_M, magnetic force strength in the axial direction;
M_T, magnetic force in the tangential direction;
M_R, magnetic Reynolds number;
T_b, Brownian motion parameter;
T_t, thermophoresis parameter;
Pr, Prandtl number;
Sc, Schmidt number;
B_n, bioconvection number;
f, axial velocity;
g, tangential velocity;
ξ, angular velocity;
b, radius of the disk;
T_{up}, dimensionless torque applied on the upper plate;
T_{low}, dimensionless torque applied on the lower plate;
$\overline{b}$, chemotaxis constant;
W_{max}, maximal speed;
D_{mo}, diffusivity of microorganisms;
R_Q, squeeze Reynolds number.

1 Introduction

Nanofluids are synthesized by adding solid particles at nanoscale to the base fluids such as ethylene glycol and water. Nanofluids have been proposed first by Eastman and Choi[1] and have been widely studied experimentally and numerically. They are applicable to many engineering problems such as heat exchangers, digital cooling systems, and chemical operations. Pak and Cho[2] determined the turbulent friction and heat transfer phenomena of the scattering fluid in a circular duct. Lin and and Yang[3] conducted a brief analysis of the flow instability of nanofluids, i.e., hydrodynamics and thermal instability. Das et al.[4] presented a detailed study on the enrichment of thermal conductivity of nanofluids. Xuan and Roetzel[5] discussed two different ways of comparing the heat transfer in nanofluids. Gherasim et al.[6] examined experimentally the heat transfer rate in the coolants filled with nanoparticles, and showed that nanofluids affected the heat transfer rate in a radial flow cooling system. Zhang et al.[7] studied the thermal diffusiveness and active thermal conductivity quantities of different nanofluids with the short-wire transitory technique. Hamilton and Crosser[8] proposed a theoretical formula for the prediction of the thermal conductivity of nanofluids. Sheikholeslami et al.[9] simulated the magnetohydrodynamics (MHD) flow of the Al-water nanofluid along with the effects of radiation and free convection.

MHD has been a vibrant topic, and has significant engineering applications such as petroleum engineering, plasma experiments, geothermal energy abstractions, and aerodynamics. The magnetic properties of fluids under electric forces are known as MHD. Many artificial approaches have been developed to examine the behaviors of boundary layers with MHD. Fakour et al.[10] deliberated the existence of a transverse magnetic field on the laminar flow with energy transfer throughout channels having porous walls. Ellahi et al.[11] studied the thermally charged two-phase flow of non-Newtonian nanofluids with particle slips and MHD. Zhu et al.[12] theoretically investigated the heat transfer rate over an annulus filled with magnetized nanofluids under slip effects. Baskaya et al.[13] examined the ferro-fluid flow, and analyzed the entropy over an inclined channel with a pressure gradient under the magnetic field effects. They showed that the entropy generation was the minimum when the magnetic field angle was perpendicular to the channel. Hamid et al.[14] used the wavelet approach to study the effects of the natural convection stagnation point flow of the Williamson fluid via the Brownian motion. Zeeshan et al.[15] addressed the entropy of the radiative flow of TiO_2-water nanofluids under the electromagnetic effects. Imtiaz et al.[16] addressed the melting heat transfer in the MHD nanofluid flow through a rotating disk. Hussain et al.[17] discussed an innovative scheme for treating lethal conditions, i.e., rheumatoid arthritis and tumors through the suspension of gold nanoparticles. Ellahi et al.[18] deliberated the flow of the natural convective mechanism along an inverted cone

with entropy generation. Heidary et al.[19] investigated numerically the thermal heat transfer of the nanofluid flow in a straight channel under the magnetic effects. They showed that the heat transfer in the presence of nanoparticles and magnetic fields in channels could be increased up to 75%. The suggested approach in his research can provide a procedure for the industrial applications for cooling and heating without growing the region of the air interchanger. Lin et al.[20–22] studied the friction factor and pressure drop with heat transfer in nanofluids.

Due to the significant attraction of squeeze flow in engines and technological processes, many researchers carried out investigations in the squeeze flow with different geometrical shapes. Sobamowo et al.[23] studied the two-dimensional (2D) squeeze nanofluid flow under a uniform transverse magnetic field and the slip boundary conditions with a variety-of-parameter method. The approximated solutions for the variations of parameters demonstrated outstanding accuracy and precision with the shooting method coupled with the Runge-Kutta method. They found that the fluid velocity increased under the slip conditions whereas showed converse behaviors with the magnetic effects. Vajravelu et al.[24] explored the flow between two squeeze parallel disks on time-dependent magnetized nanofluids with transpiration, speed slip, and temperature slip. Hosseinzadeh et al.[25] investigated the heat and mass transfer between two parallel plates filled with magnetized nanofluids. Hashmi et al.[26] discussed the nanofluid stream around parallel disks with the magnetized squeeze motion, and used the homotopy analysis method to construct analytical representations for the velocity, nanoparticle concentration, and temperature. Singh et al.[27] considered the uniform magnetic field with the thermal and mass transfer mechanism of the unstable squeeze nanofluid flow between two plates, and indicated that with increases in the Schmidt number and squeeze parameter, the frequency of mass transfer increased. Bhatta et al.[28] considered the squeeze flow among two parallel disks filled with water-based nanofluids. Madaki et al.[29] studied the presence of thermal radiation between two lateral plates with unstable squeeze nanofluid flow. Vimala and Manimegalai[30] proposed an energy integral method for the laminar squeeze flow of Cu-water and Al-water nanofluids between circular disks. Acharya et al.[31] examined the squeeze flow and magnetic field between two plates filled with Cu-water and Cu-kerosene nanofluids, and showed that the fluid rate decreased when the Hartmann number and squeeze parameter increased while the fluid speed in the same region increased when the particle volume fraction of nanoparticles increased. Thongmoon and Pusjuso[32] presented a one-dimensional (1D) differential transform scheme and examined the exact solution to the system ordinary differential equations. Fatoorehchi and Abolghasemi[33] used the differential transform method (DTM) to examine the mass transfer flow through a thin liquid film. Yousif et al.[34] studied the Casson fluid flow through a flat porous plate under a magnetic field with the differential transformation method along with the Padé approximation. Çilingir et al.[35] examined the constant laminar flow of a 2D electrically conducting viscous fluid through an exponentially stretching surface.

Bioconvection results due to microorganisms, which are denser than water and swim generally in an upward direction. When the upper surface is denser enough due to the suspension of microorganisms, it will become unstable and the microorganisms will collapse and cause bioconvection. Gyrotactic microorganisms (a characteristic of many algae species) swim in still water against gravity. But once bioconvection occurs, the balance of two torques, i.e., the viscous torque of a body placed in the shear flow and the torque produced by gravity due to the mass of a typical alga separated from its buoyancy center, decides the swimming guidelines. Many significant results have been obtained in the field of bioconvection over the past few years. Khan et al.[36] provided a mathematical model to investigate the natural convection boundary layer flow over a truncated cone under convective surface boundary conditions with gyrotactic micro-organisms in a water-based nanofluid. Saleem et al.[37] studied the behavioral feature of gyrotactic microorganisms on a Jeffery MHD nanofiuid. Khan et al.[38] studied the effects of the Navier slip and magnetic field on the movement of the boundary layer with heat and mass transfer of water-based nanofluids filled with gyrotactic microorganisms over a vertical plate. Farooq

et al.[39] discussed numerically the gyrostatic microorganisms in the flow of a mixed convective non-Newtonian Sisko nanofluid. Waqas et al.[40–41] considered the flow of nanofluids over a stretching surface with heat transfer, mass transfer, and motile microorganisms in the presence of time-dependent MHD with a numerical scheme. Aziz et al.[42] studied the continuous boundary surface of the free convection glide embedded in a porous medium through a horizontal flat plate containing water-based nanofluids and gyrotactic microorganisms. Raees et al.[43] elaborated the mixed convection gravitational flow with microorganisms and nanoparticles. Meade et al.[44] performed numerical simulations of water-based ZnO nanofluids containing rod-like nanoparticles in turbulent and laminar pipe flow.

In the present investigation, we consider the swimming of microorganisms and the movement of nanoparticles through rotating circular plates via a generalized magnetic Reynolds number. The nanoparticles are suspended in the circular finite rotating plates with gyrotactic microorganisms. The induced magnetic field phenomena in the tangential and azimuthal directions are considered in the present mathematical formulation. The governing nonlinear partial differential equations are firstly converted by applying similarity transformations into the set of nonlinear ordinary differential equations. The resulting nonlinear system of highly nonlinear coupled ordinary differential equations is then solved through the DTM-Padé method. The behaviors of different factors on the velocity, induced MHD, temperature, microorganism density, and nanoparticle concentration are analyzed in detail.

2 Mathematical modeling

We assume the axisymmetric flow of a squeeze lubricant film between a pair of two finite parallel circular plates. We consider the polar coordinate (r, θ, z) system and the velocity U with the components u, v, and w corresponding to the r-, θ-, and z-directions, respectively. The plates are connected with a height $\Gamma(t)$ $(= (1 - \beta t)^{1/2} D)$ at the time t, where D indicates the representative length. Assume that the upper plate is moving with the velocity $\Gamma'(t)$ towards the lower plate, while the lower plate is fixed. The z-axis represents the axis of symmetry, about which both plates are rotating. The upper plate is under the effect of an external magnetic field (applied) H with the axial and azimuthal components as follows:

$$H_\theta = \frac{rN_0}{\mu_2}\sqrt{\frac{D}{\Gamma(t)}}, \quad H_z = \frac{\alpha M_0 D}{\mu_1 \Gamma(t)}, \tag{1}$$

where M_0 and N_0 are the dimensionless quantities making H_θ and H_z dimensionless, respectively, and μ_1 and μ_2 are the magnetic permeabilities inside and outside the plate, respectively. For the liquid metals, $\mu_2 = \mu_{\mathrm{f}}$, where μ_{f} represents the free space permeability. H_θ and H_z on the lower plate are presumed to be zero. The magnetic field (applied) generates a magnetic field (induced) $B(r, \theta, z)$ having the components B_r, B_θ, and B_z in the squeeze film among the plates (see Fig. 1). The lower and upper plates are retained at a constant temperature (T_{l}, T_{u}) and concentration (C_{l}, C_{u}). We consider that the electrically conducting fluid contains nanoparticles and gyrotactic microorganisms. With the above assumptions, the equations of continuity and momentum for the hydro-magnetic squeeze film regime read as

$$\nabla \cdot U = 0, \tag{2}$$

$$\rho\Big((U \cdot \nabla)U + \frac{\partial U}{\partial t}\Big) - \mu \nabla^2 U + \nabla p - \frac{1}{\mu_2}\big((\nabla \times B) \times B\big) = 0, \tag{3}$$

where p is the pressure, ρ is the fluid density, and μ is the fluid viscosity. The magnetic field equations read as

$$\nabla \cdot B = 0, \tag{4}$$

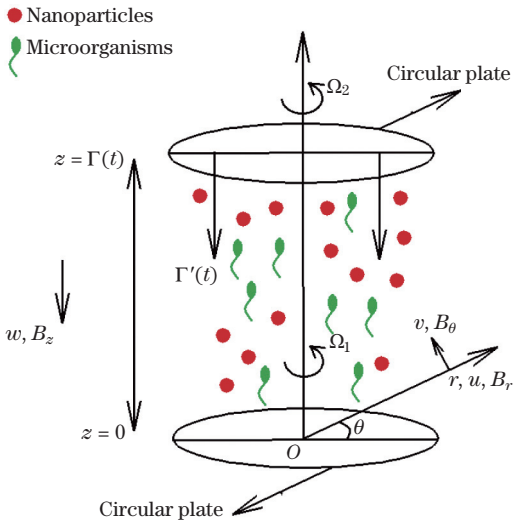

Fig. 1 Schematic diagram of nanoparticles between parallel finite plates in the presence of microorganisms (color online)

$$\frac{\partial B}{\partial t} - \nabla \times (U \times B) = \frac{1}{\delta \mu_2} \nabla^2 B, \tag{5}$$

where δ is the electrical conductivity. The energy equation reads as

$$(U \cdot \nabla) T - \frac{1}{\rho c_p} \nabla \cdot (k \nabla) T + \tau \left(D_{\mathrm{B}} \nabla T \cdot \nabla C + \left(\frac{D_{\mathrm{T}}}{T_{\mathrm{m}}} \right) \nabla T \cdot \nabla T \right) = 0, \tag{6}$$

where T is the temperature, C is the concentration, T_{m} is the mean fluid temperature, c_p is the specific heat at uniform temperature, D_{B} is the Brownian diffusivity, and D_{T} is the thermophoretic diffusion coefficient.

The nanoparticle concentration equation reads as

$$(U \cdot \nabla) C - D_{\mathrm{c}} \nabla \cdot (\nabla \cdot C) - \frac{D_{\mathrm{T}}}{T_{\mathrm{m}}} \nabla \cdot (\nabla \cdot T) = 0, \tag{7}$$

where D_{c} is the diffusion coefficient. The microorganism conservation reads as

$$\frac{\partial n}{\partial t} + \nabla \cdot j = 0, \tag{8}$$

where j is the microorganism flux due to the fluid convection, and

$$j = nV + n\psi - D_{\mathrm{mo}} \nabla \cdot n. \tag{9}$$

The average form of the directional swimming velocity of a microorganism reads as

$$\psi = \overline{b} W_{\max} H(C) \nabla \cdot C, \tag{10}$$

where $\overline{b}$ and $W_{\max}$ are the chemotaxis constant and the maximal speed of the cell swimming, respectively, $\overline{b} W_{\max}$ is considered as a constant, $H(C)$ is the Heaviside step function which is considered to unity here, and the diffusivity of microorganisms is denoted by D_{mo}.

The corresponding boundary conditions are as follows.

At $z = 0$,

$$\begin{cases} u = 0, \quad v = \Omega_1 r \dfrac{D^2}{\Gamma^2(t)}, \quad w = 0, \\ B_z = B_\theta = 0, \quad C = C_\mathrm{l}, \quad T = T_\mathrm{l}, \quad n = n_\mathrm{l}. \end{cases} \tag{11}$$

At $z = \Gamma(t)$,

$$\begin{cases} u = 0, \quad v = \Omega_2 r \dfrac{D^2}{\Gamma^2(t)}, \quad w = -\dfrac{\beta D^2}{2\Gamma(t)}, \quad B_\theta = N_0 r \dfrac{D^2}{\Gamma^2(t)}, \\ B_z = -\dfrac{\beta D M_0}{\Gamma(t)}, \quad T = T_\mathrm{u}, \quad C = C_\mathrm{u}, \quad n = n_\mathrm{u}, \end{cases} \tag{12}$$

where Ω_1 and Ω_2 are angular velocities, and n_u represents the microorganism at the upper plate.

2.1 Similarity transformations

Introduce the following similarity transformations:

$$\begin{cases} u = r\dfrac{\partial F}{\partial z} = \dfrac{\beta r}{2}\dfrac{D^2}{\Gamma^2(t)}\dfrac{\mathrm{d}f}{\mathrm{d}\lambda}, \quad v = rG(z,t) = r\Omega_1 \dfrac{D^2}{\Gamma^2(t)} g(\lambda), \\ w = -2F(z,t) = -\dfrac{\beta D^2 f(\lambda)}{\Gamma(t)}, \quad B_r = r\dfrac{\partial M}{\partial z} = \dfrac{\beta r D M_0}{2\Gamma^2(t)}\dfrac{\mathrm{d}m}{\mathrm{d}\lambda}, \\ B_\theta = rN(z,t) = rN_0 \dfrac{D^2}{\Gamma^2(t)} n(\lambda), \quad B_z = -2M(z,t) = -\dfrac{\beta D M_0 m(\lambda)}{\Gamma(t)}, \\ \phi(\lambda) = \dfrac{C - C_\mathrm{u}}{C_\mathrm{l} - C_\mathrm{u}}, \quad \chi(\lambda) = \dfrac{n - n_\mathrm{u}}{n_\mathrm{l} - n_\mathrm{u}}, \quad \theta(\lambda) = \dfrac{T - T_\mathrm{u}}{T_\mathrm{l} - T_\mathrm{u}}, \quad \lambda = \dfrac{z}{\Gamma(t)}. \end{cases} \tag{13}$$

Substituting the above similarity transformations into Eqs. (2)–(10), we obtain the following set of coupled ordinary differential equations with the single-spaced variable λ:

$$f'''' = R_\mathrm{Q}\Big(3f'' - 2\Big(\frac{R_\mathrm{M}}{R_\mathrm{Q}}\Big)^2 gg' + 2M_\mathrm{T}^2\big(mm''' + m'm''\big) - \big(2f - \lambda\big)f''' + 2N_\mathrm{T}^2\Big(\frac{R_\mathrm{M}}{R_\mathrm{Q}}\Big)^2 nn'\Big), \tag{14}$$

$$g'' = R_\mathrm{Q}\big(2g + \lambda g' + 2gf' - fg' + 2N_\mathrm{T}M_\mathrm{T}\big(mn' + nm'\big)\big), \tag{15}$$

$$m'' = M_\mathrm{R}\big(m + \lambda m' - 2fm' + 2mf'\big), \tag{16}$$

$$n'' = M_\mathrm{R}\Big(2n + \lambda n' + 2\Big(\frac{N_\mathrm{T}}{M_\mathrm{T}}\Big)mg' - fn'\Big), \tag{17}$$

$$\theta'' + T_\mathrm{b}\theta'\phi' + T_\mathrm{t}\theta'^2 + R_\mathrm{Q}Prf\theta' = 0, \tag{18}$$

$$\phi'' + \frac{T_\mathrm{t}}{T_\mathrm{b}}\theta'' + R_\mathrm{Q}Scf\phi' = 0, \tag{19}$$

$$\chi'' - R_\mathrm{Q}B_\mathrm{n}\Big(\frac{\lambda}{2}\Big)\chi' + B_\mathrm{n}R_\mathrm{Q}f\chi' - Pe\big(\chi'\phi' + (\chi + \Phi)\phi''\big) = 0, \tag{20}$$

where R_Q is the squeeze Reynolds number, R_M is the magnetic force strength in the axial direction, M_T is the magnetic force in the tangential direction, M_R is the magnetic Reynolds number, T_b is the Brownian motion parameter, T_t is the thermophoresis parameter, Pr is the Prandtl number, Sc is the Schmidt number, B_n is the bioconvection number, and Φ is the

constant number. They are defined as follows:

$$\begin{cases} R_{\mathrm{Q}}=\dfrac{\alpha D^2}{2\upsilon}, \quad R_{\mathrm{M}}=\dfrac{\Omega_1 D^2}{\upsilon}, \quad M_{\mathrm{T}}=\dfrac{M_0}{D\sqrt{\mu_2\rho}}, \quad N_{\mathrm{T}}=\dfrac{N_0}{\Omega_1\sqrt{\mu_2\rho}}, \\ T_{\mathrm{b}}=\dfrac{\tau D_{\mathrm{B}}(C_{\mathrm{l}}-C_{\mathrm{u}})}{\alpha}, \quad T_{\mathrm{t}}=\dfrac{\tau D_{\mathrm{T}}(T_{\mathrm{l}}-T_{\mathrm{u}})}{\alpha}, \quad Pr=\dfrac{\upsilon}{\alpha}, \quad Sc=\dfrac{\upsilon}{D_{\mathrm{B}}}, \\ B_{\mathrm{n}}=\dfrac{\upsilon}{D_n}, \quad Pe=\dfrac{\overline{b}W_{\max}}{D_{\mathrm{mo}}}, \quad \Phi=\dfrac{n_\infty}{n_{\mathrm{w}}-n_\infty}, \quad \alpha=\dfrac{k}{\rho c_p}, \quad Bt=\delta\mu_2\upsilon, \quad M_{\mathrm{R}}=R_{\mathrm{Q}}Bt, \end{cases} \tag{21}$$

in which "Bt" is the Batchelor number.

The corresponding boundary conditions read as

$$\begin{cases} f(0)=0, \quad f'(0)=0, \quad g(0)=1, \quad m(0)=0, \quad n(0)=1, \\ \theta(0)=1, \quad \chi(0)=1, \quad \phi(0)=1, \quad f(1)=\dfrac{1}{2}, \quad g(1)=\xi, \\ m(1)=1, \quad n(1)=1, \quad \theta(1)=0, \quad \phi(1)=0, \quad \chi(1)=0, \end{cases} \tag{22}$$

where f and g are the axial and tangential velocities, respectively, m and n are the axial and tangential induced magnetic field components, respectively, θ is the temperature function of nanoparticles, ϕ is the concentration function of the nanoparticle volume fraction, χ is the motile microorganism density function, and ξ $(=\Omega_2/\Omega_1)$ represents the corresponding angular velocity between the plates having a range of $-1 \leqslant \xi \leqslant 1$, which is beneficial to examine different flow features associated with the plates rotating in the opposite and same directions.

The non-dimensional torque applied on the upper plate can be calculated by

$$T_{\mathrm{up}}=2\pi\rho\int_0^b \Big(\frac{\partial v}{\partial z}\Big)_{z=\Gamma(t)}\mathrm{d}r, \tag{23}$$

where b is the radius of the disk.

Substituting Eq. (13) into Eq. (23), we get

$$T_{\mathrm{up}}=\frac{\mathrm{d}g(1)}{\mathrm{d}\lambda}, \tag{24}$$

where T_{u} is the dimensionless torque applied on the upper plate by the fluid, and $\mathrm{d}g(1)/\mathrm{d}\lambda$ is the tangential velocity gradient on the upper plate.

Similarly, the dimensionless torque for the lower plate is given by the same calculation at $\lambda=0$. We have

$$T_{\mathrm{low}}=\frac{\mathrm{d}g(0)}{\mathrm{d}\lambda}. \tag{25}$$

3 Proposed method: DTM

The DTM is based on the Taylor series expansion. It provides an analytical solution in the form of a polynomial. The MHD and complex material flow problems can be solved by using the DTM, which is a reliable technique in finding the solutions to nonlinear problems. To explain briefly the DTM method, let us define the qth derivative as follows:

$$F(\lambda)=\frac{1}{q!}\Big(\frac{\mathrm{d}^q f}{\mathrm{d}\lambda^q}\Big)_{\lambda=\lambda_0}, \tag{26}$$

where $f(\lambda)$ and $F(\lambda)$ represent the original and transformed functions, respectively. We can define the differential inverse transformation of $F(\lambda)$ as follows:

$$f(\lambda)=\sum_{q=0}^{\infty}F(\lambda)(\lambda-\lambda_0)^q. \tag{27}$$

With differential transformations, the function $f(\lambda)$ can be written in terms of a finite series as follows:

$$f(\lambda) \cong \sum_{q=0}^{k} F(\lambda)(\lambda - \lambda_0)^q. \tag{28}$$

The convergence rate depends upon the value of k.

Substituting the differential transformations of Eq. (26) into Eqs. (14)–(20), we get

$$\begin{aligned} f(q+4) =& \frac{R_{\mathrm{Q}}}{(q+4)(q+3)(q+2)(q+1)}\big(3(1+q)(2+q)f(2+q)\big) \\ &+ \sum_{i=0}^{q}\big((1-i+q)(2-i+q)(3-i+q)\varepsilon(i)f(3-i+q)\big) \\ &- \sum_{i=0}^{q}\big(2(1-i+q)(2-i+q)(3-i+q)f(i)f(3-i+q)\big) \\ &- 2\frac{R_{\mathrm{M}}^2}{R_{\mathrm{Q}}^2}\sum_{i=0}^{q}\big((1-i+q)g(i)g(1-i+q)\big) \\ &+ 2M_{\mathrm{T}}^2\sum_{i=0}^{q}(1-i+q)(2-i+q)(3-i+q+)m(i)m(3-i+q) \\ &+ (1+i)(i+2)(1-i+q)(2-i+q)m(i+1)m(2-i+q) \\ &+ 2N_{\mathrm{t}}^2\Big(\frac{R_{\mathrm{M}}^2}{R_{\mathrm{Q}}^2}\Big)^2\sum_{i=0}^{q}\big((q-i+1)n(q+1-i)n(i)\big), \end{aligned} \tag{29}$$

$$\begin{aligned} g(q+2) =& \frac{R_{\mathrm{Q}}}{(q+2)(q+1)}\Big(2g(q) + \sum_{i=0}^{q}\big((1-i+q)+\varepsilon(i)g(1-i+q)\big) \\ &+ \sum_{i=0}^{q}\big(2(1-i+q)g(i)f(1-i+q) - 2\big(1-i+q\big)f(i)g(1-i+q)\big) \\ &+ 2N_{\mathrm{T}}M_{\mathrm{T}}\sum_{i=0}^{q}\big((1-i+q)m(i)n(1-i+q) - (1-i+q)n(i)m(1-i+q)\big)\Big), \end{aligned} \tag{30}$$

$$\begin{aligned} m(q+2) =& \frac{M_{\mathrm{R}}}{(q+1)(q+2)}\Big(m(q) + \sum_{i=0}^{p}(1-i+q)\varepsilon(i)m(1-i+q) \\ &- \sum_{i=0}^{q}\big(2(1-i+q)f(i)m(1-i+q) - 2(1-i+q)m(i)f(1-i+q)\big)\Big), \end{aligned} \tag{31}$$

$$\begin{aligned} n(q+2) =& \frac{M_{\mathrm{R}}}{(q+1)(q+2)}\Big(2n(q) + \sum_{i=0}^{p}(1-i+q)\varepsilon(i)n(1-i+q) \\ &- \sum_{i=0}^{p}\Big(2(1-i+q)f(i)n(1-i+q) - 2\Big(\frac{N_{\mathrm{T}}}{M_{\mathrm{T}}}\Big)(1-i+q)g(1-i+q)m(i)\Big)\Big), \end{aligned} \tag{32}$$

$$\theta(q+2) = \frac{Pr}{(q+1)(q+2)}\Big(-R_{\mathrm{M}}\sum_{i=0}^{q}(1-i+q)f(i)\theta(1-i+q) - \sum_{i=0}^{q}T_{\mathrm{t}}(1+i)(1-i+q)\theta(1+i)\theta(1-i+q) - \sum_{i=0}^{p}T_{\mathrm{b}}(1+i)(1-i+q)\phi(1-i+q)\theta(i+1)\Big), \tag{33}$$

$$\phi(q+2) = \frac{1}{(q+1)(q+2)}\Big(-R_{\mathrm{Q}}Sc\sum_{i=0}^{q}(1-i+q)f(i)\phi(1-i+q) - \Big(\frac{T_{\mathrm{t}}}{T_{\mathrm{b}}}\Big)\theta(q+2)(2+q)(1+q)\Big), \tag{34}$$

$$\chi(q+2) = \frac{1}{(1+q)(2+q)}\Big(R_{\mathrm{Q}}Sc\sum_{i=0}^{q}\frac{\varepsilon(i)}{2}(q+1-i)\chi(1-i+q) - R_{\mathrm{Q}}Sc\sum_{i=0}^{q}(1-i+q)f(i)\chi(1-i+q) + Pe\Big(\sum_{i=0}^{q}(i+1)(1-r+q)\chi(1+i)\phi(q+1-i) + \sum_{i=0}^{q}\big((1-i+q)(2-i+q)\chi(i)\phi(2-i+q) + \big(\chi(i)+\Phi\big)(1+Q)(2+q)\phi(2+q)\big)\Big)\Big), \tag{35}$$

where $f(q)$, $g(q)$, $m(q)$, $n(q)$, $\theta(q)$, $\phi(q)$, and $\chi(q)$ are the differential transformations of $f(\lambda)$, $g(\lambda)$, $m(\lambda)$, $n(\lambda)$, $\theta(\lambda)$, $\phi(\lambda)$, and $\chi(\lambda)$, respectively, which are defined by

$$f(\lambda) = \sum_{q=0}^{\infty} f(q)\lambda^q, \tag{36}$$

$$g(\lambda) = \sum_{q=0}^{\infty} g(q)\lambda^q, \tag{37}$$

$$m(\lambda) = \sum_{q=0}^{\infty} m(q)\lambda^q, \tag{38}$$

$$n(\lambda) = \sum_{q=0}^{\infty} n(q)\lambda^q, \tag{39}$$

$$\theta(\lambda) = \sum_{q=0}^{\infty} \theta(q)\lambda^q, \tag{40}$$

$$\phi(\lambda) = \sum_{q=0}^{\infty} \phi(q)\lambda^q, \tag{41}$$

$$\chi(\lambda) = \sum_{q=0}^{\infty} \chi(q)\lambda^q. \tag{42}$$

The boundary conditions are

$$\begin{cases} f(0) = 0, \quad f(1) = \dfrac{1}{2}, \quad g(0) = 1, \quad m(0) = 0, \quad n(0) = 0, \\ \theta(0) = 1, \quad \phi(0) = 0, \quad \chi(0) = 0, \quad f(2) = \alpha_1, \quad f(3) = \alpha_2, \quad g(1) = \alpha_3, \\ m(1) = \alpha_4, \quad n(1) = \alpha_5, \quad \theta(1) = \alpha_6, \quad \phi(1) = \alpha_7, \quad \chi(1) = \alpha_8, \end{cases} \tag{43}$$

where α_i $(i = 1, 2, 3, \cdots, 8)$ are constants. By replacing Eq. (43) into Eqs. (26)–(32), we obtain the expressions for $f(\lambda)$, $g(\lambda)$, $m(\lambda)$, $n(\lambda)$, $\theta(\lambda)$, $\phi(\lambda)$, and $\chi(\lambda)$ in the simplified forms as follows:

$$f(\lambda) = f_1\lambda^2 + f_2\lambda^3 + f_3\lambda^4 \cdots, \tag{44}$$

$$g(\lambda) = 1 - g_1\lambda + g_2\lambda^2 + \cdots, \tag{45}$$

$$m(\lambda) = m_1\lambda + m_2\lambda^3 + m_3\lambda^4 + \cdots, \tag{46}$$

$$n(\lambda) = n_1\lambda + n_2\lambda^3 + n_3\lambda^4 + \cdots, \tag{47}$$

$$\theta(\lambda) = 1 + \theta_1\lambda + \theta_2\lambda^2 + \cdots, \tag{48}$$

$$\phi(\lambda) = 1 + \phi_1\lambda + \phi_2\lambda^2 + \cdots, \tag{49}$$

$$\chi(\lambda) = 1 + \chi_1\lambda + \chi_2\lambda^2 + \cdots, \tag{50}$$

where f_i, g_i, m_i, n_i, θ_i, ϕ_i, and χ_i $(i = 1, 2, 3, \cdots)$ are constants with long and complex values which are difficult to express here. We solve these equations by using the Mathematica software with 30 iterations. But the convergence rate is prolonged. For a more and accurate convergence radius, the Padé approximation is used, because without the Padé approximation, the DTM is not able to fulfill the conditions.

3.1 Padé approximation

The Padé approximation helps to increase the convergence rate of the resulting polynomial equations. The analytical solution achieved by the DTM cannot meet the boundary condition at $\lambda = 1$ without applying the Padé approximation. Thus, the series solution obtained by the DTM with the Padé approximation must be merged to achieve a useful tool to resolve the boundary value problem.

Let us consider the power series as follows:

$$f(\gamma) = \sum_{i=0}^{\infty} a_i\gamma^i. \tag{51}$$

The rational fraction is known as the Padé approximation, i.e.,

$$[L/K] = \frac{D_L(\gamma)}{E_K(\gamma)}, \tag{52}$$

where $D_L(\gamma)$ is a polynomial of degree at most L, and $E_K(\gamma)$ is a polynomial of degree at most K. Therefore,

$$f(\gamma) = a_0 + a_1\gamma + a_2\gamma^2 + a_3\gamma^3 + \cdots, \tag{53}$$

$$D_L(x) = D_0 + D_1\gamma + D_2\gamma^2 + \cdots + D_L\gamma^L, \tag{54}$$

$$E_K(\gamma) = E_0 + E_1\gamma + E_2\gamma^2 + \cdots + E_K\gamma^L. \tag{55}$$

In Eq. (52), $L+1$ and $K+1$ are the numerator and denominator coefficients, respectively. Since the denominator and numerator can be multiplied by a constant and $[L/K]$ remains unaffected, the following normalization condition is imposed:

$$E_K(0) = 1. \tag{56}$$

Thus, we have $L+1$ and K independent numerator and denominator coefficients, respectively, which make all the coefficients $L+K+1$ unknown. This number suggests that, usually, Eq. (51) ought to fit the power series of Eq. (50) through the order 1, γ, γ^2, γ^3, $\cdots$, γ^{L+K} in the notation of the formal power series as follows:

$$\sum_{i=0}^{\infty} a_i\gamma^i = \frac{D_0 + D_1\gamma + D_2\gamma^2 + \cdots + D_L\gamma^L}{E_0 + E_1\gamma + E_2\gamma^2 + \cdots + E_K\gamma^K} + O(\gamma^{L+K+1}). \tag{57}$$

By cross multiplying Eq. (57), we get

$$\begin{aligned} &\left(E_0 + E_1\gamma + E_2\gamma^2 + \cdots + E_K\gamma^K\right) \times \left(a_0 + a_1\gamma + a_2\gamma^2 + \cdots\right) \\ &= (D_0 + D_1\gamma + D_2\gamma^2 + \cdots + D_L\gamma^L) + O(\gamma^{L+K+1}). \end{aligned} \tag{58}$$

Equating the coefficients of γ^{L+1}, γ^{L+2}, $\cdots$, γ^{L+K}, we get

$$\begin{cases} E_K a_{L-K+1} + E_{K-1}a_{L-K+2} + \cdots + E_0 a_{L+1} = 0, \\ E_K a_{L-K+2} + E_{K-1}a_{L-K+3} + \cdots + E_0 a_{L+2} = 0, \\ \qquad\qquad \vdots \\ E_K a_{\text{l}} + E_{K-1}a_{L+1} + \cdots + E_0 a_{L+K} = 0. \end{cases} \tag{59}$$

If $j < 0$, we define $a_j = 0$ for consistency. Since $E_0 = 1$, Eq. (59) becomes a set of K linear equations for the K unknown denominator coefficients as follows:

$$\begin{pmatrix} a_{L+1-K} & a_{L+2-K} & a_{L+3-K} & \cdots & a_{\text{l}} \\ a_{L+2-K} & a_{L+3-K} & a_{L+4-K} & \cdots & a_{L+1} \\ a_{L+3-K} & a_{L+4-K} & a_{L+5-K} & \cdots & a_{L+2} \\ \vdots & \vdots & \vdots & & \vdots \\ a_{\text{l}} & a_{1+L} & a_{2+L} & \cdots & a_{L+1-K} \end{pmatrix} \begin{pmatrix} E_K \\ E_{K-1} \\ E_{K-2} \\ \vdots \\ E_1 \end{pmatrix} = - \begin{pmatrix} a_{L+1} \\ a_{L+2} \\ a_{L+3} \\ \vdots \\ a_{L+K} \end{pmatrix}. \tag{60}$$

E_i can be determined from these equations. The numerator coefficients f_0, f_1, f_2, $\cdots$, f_l are immediately obtained from Eq. (58) with equating the coefficients of 1, γ, γ^2, $\cdots$, γ^{L+K} as follows:

$$f_0 = a_0, \tag{61}$$

$$f_1 = a_1 + G_1 a_0, \tag{62}$$

$$f_2 = a_2 + G_1 a_1 + G_2 a_0, \tag{63}$$

$$\vdots \tag{64}$$

$$f_l = a_l + \sum_{i=1}^{\min[L,K]} E_i a_{L-i}. \tag{65}$$

Equations (59)–(60) help typically to examine the Padé denominator and numerator, and are known as the Padé equations.

The Padé approximant $[L, K]$ is formulated, which satisfies $\sum_{i=0}^{\infty} a_i \gamma^i$ through the order γ^{L+K}. The Padé approximants of Eqs. (43)–(49) are as follows:

$$f(\lambda)=\frac{-1.503\ 66\lambda^2-0.533\ 47\lambda^3+0.343\ 571\lambda^4+0.009\ 470\ 01\lambda^5+\cdots}{1-0.325\ 734\lambda-0.026\ 573\ 9\lambda^2+0.003\ 392\ 43\lambda^3-0.000\ 458\ 943\lambda^4+0.000\ 349\ 636\lambda^5+\cdots}, \quad (66)$$

$$g(\lambda)=\frac{1-1.322\ 74\lambda+0.236\ 91\lambda^2-0.014\ 724\ 7\lambda^3+0.038\ 065\ 3\lambda^4+0.060\ 191\ 4\lambda^5+\cdots}{1-0.375\ 403\lambda-0.218\ 721\lambda^2-0.036\ 775\ 8\lambda^3-0.006\ 226\ 23\lambda^4+0.002\ 319\ 95\lambda^5+\cdots}, \quad (67)$$

$$m(\lambda)=\frac{1.733\ 69\lambda+4.650\ 46\lambda^2-1.760\ 21\lambda^3+0.727\ 911\lambda^4-4.193\ 17\lambda^5+\cdots}{1+2.682\ 4\lambda-1.515\ 3\lambda^2-0.545\ 426\lambda^3-0.495\ 658\lambda^4+0.151\ 876\lambda^5+\cdots}, \quad (68)$$

$$n(\lambda)=\frac{1.127\ 35\lambda+0.356\ 725\lambda^2+0.170\ 818\lambda^3-0.046\ 669\ 8\lambda^4-0.475\ 831\lambda^5+\cdots}{1+0.316\ 428\lambda+0.129\ 949\lambda^2-0.501\ 031\lambda^3-0.518\ 327\lambda^4-0.236\ 133\lambda^5+\cdots}, \quad (69)$$

$$\theta(\lambda)=\frac{1-3.345\ 04\lambda+3.003\ 36\lambda^2-1.453\ 87\lambda^3+0.593\ 719\lambda^4-0.236\ 454\lambda^5+\cdots}{1-1.70091\lambda+1.2924\lambda^2-0.697\ 595\lambda^3+0.334\ 838\lambda^4-0.081\ 230\ 5\lambda^5+\cdots}, \quad (70)$$

$$\phi(\lambda)=\frac{1-1.136\ 57\lambda+1.568\ 23\lambda^2-0.693\ 967\lambda^3+0.269\ 388\lambda^4-0.007\ 145\ 46\lambda^5+\cdots}{1-0.838\ 759\lambda+0.232\ 89\lambda^2-0.191\ 925\lambda^3+0.081\ 022\ 9\lambda^4+0.023\ 184\ 5\lambda^5+\cdots}, \quad (71)$$

$$\chi(\lambda)=\frac{1-1.287\ 83\lambda+1.033\ 47\lambda^2-0.654\ 857\lambda^3+0.397\ 859\lambda^4-0.018\ 948\ 9\lambda^5+\cdots}{1-0.771\ 776\lambda-0.538\ 057\lambda^2+0.001\ 792\ 18\lambda^3+0.255\ 265\lambda^4+0.109\ 99\lambda^5+\cdots}. \quad (72)$$

4 Numerical results, validation, and discussion

In this section, we discuss the numerical results obtained by a computational software Mathematica of DTM-Padé, which has been used successfully to find the analytical solution to coupled nonlinear differential equations for the governing flow. The effects of different parameters such as the squeeze Reynolds number R_{Q}, the magnetic forces in the axial and tangential directions R_{M} and M_{T}, the magnetic Reynolds number M_{R}, and the induced magnetic field components m and n are discussed. The effects of the Prandtl number Pr, Brownian motion parameter T_{b}, thermophoresis parameter T_{t}, Schmidt number Sc, bioconvection number B_{n}, and Peclet number Pe are also considered. The results are shown in Figs. 2–10.

To authenticate the exactness of our results, a comparison with the shooting method in Ref. [44] is given. The Padé approximation is used to validate the convergence of the series solutions. The results obtained by the DTM-Padé method and the shooting method for multiple values of the leading parameters are shown in Table 1. We can observe from this table that our results perfectly match with the numerical results by the shooting method.

Table 1 Values of $\theta'(0)$, $\phi'(0)$, and $\chi'(0)$ obtained by the DTM-Padé $[5\times5]$ method and the shooting method Parameter

		$\theta'(0)$		$\phi'(0)$		$\chi'(0)$	
		Shooting method	DTM-Padé	Shooting method	DTM-Padé	Shooting method	DTM-Padé
N_{t}	0.10	−0.619 650	−0.619 650	−1.922 555	−1.922 555	−1.613 755	−1.613 755
	0.20	−0.413 998	−0.413 998	−3.168 139	−3.168 139	−1.987 593	−1.987 593
N_{b}	0.10	−0.955 216	−0.955 216	−1.769 984	−1.769 984	−1.568 817	−1.568 817
	0.20	−0.680 870	−0.680 870	−1.800 588	−1.800 588	−1.580 640	−1.580 640
Pr	5.0	−0.863 804	−0.863 804	−1.511 531	−1.511 531	−1.633 151	−1.633 151
	10.0	−0.733 705	−0.733 705	−1.647 605	−1.647 605	−1.710 388	−1.710 388
R_{Q}	−2.0	−0.009 741	−0.009 741	−0.909 232	−0.909 232	−1.050 186	−1.050 186
	1.0	−0.733 705	−0.733 705	−1.512 289	−1.512 289	−1.510 372	−1.510 372
B_{n}	5.0	−0.737 106	−0.737 106	−1.511 531	−1.511 531	−1.380 064	−1.380 064
	10.0	−0.736 283	−0.736 283	−1.512 289	−1.512 289	−1.324 426	−1.324 426
Sc	5.0	−0.683 897	−0.683 897	−1.511 531	−1.511 531	−1.424 089	−1.424 089
	10.0	−0.635 811	−0.635 811	−1.844 023	−1.844 023	−1.561 973	−1.561 973

Table 2 shows the errors of the results of the DTM-Padé method and the shooting method. We can see from this table that the errors between both schemes are minimal and almost negligible, which shows that the present method used is an efficient tool to examine the highly nonlinear equations. Tables 3 and 4 reveal the torque effects on the upper and lower circular plates, which are calculated with the help of Eqs. (24)–(25).

Table 2 Errors of the shooting method and the DTM-Padé [5 × 5] method

	Shooting method	DTM-Padé [5×5]	Error
$f''(1)$	−2.997 494 629 198 898	−2.997 494 629 198 898	0
$f'''(1)$	−6.069 084 589 598 415	−6.069 084 589 598 414	-1×10^{-15}
$g'(1)$	−0.947 265 509 297 220	−0.947 265 509 297 220	0
$m'(1)$	1.523 121 281 937 509 5	1.523 121 281 937 509 5	0
$n'(1)$	1.068 831 491 459 310 7	1.068 831 491 459 310 7	0
$\theta'(1)$	−1.084 379 592 223 696	−1.084 379 592 223 696	0
$\phi'(1)$	−0.899 024 384 614 488	−0.899 024 384 614 488	-2×10^{-16}
$\chi'(1)$	−0.763 298 959 655 151	−0.763 298 959 655 151	0

Table 3 Torque values at the lower and upper plates when $R_{\mathrm{M}} = 0.3$, $M_{\mathrm{T}} = 0.5$, and $Bt = 0.6$ for various values of R_{Q}

R_{Q}	$\mathrm{d}g(0)/\mathrm{d}\lambda$		$\mathrm{d}g(1)/\mathrm{d}\lambda$	
	DTM-Padé	Shooting method	DTM-Padé	Shooting method
0.1	−1.092 937 221 430 923	−1.092 937 221 430 923	−0.948 663 684 660 318	−0.948 663 684 660 318
0.2	−1.180 889 912 821 983	−1.180 889 912 821 983	−0.901 360 783 950 894	−0.901 360 783 950 894

Table 4 Torque values at the lower and upper plates when $R_{\mathrm{Q}} = 0.3$, $M_{\mathrm{T}} = 0.5$, and $Bt = 0.6$ for various values of R_{M}

R_{M}	$\mathrm{d}g(0)/\mathrm{d}\lambda$		$\mathrm{d}g(1)/\mathrm{d}\lambda$	
	DTM-Padé	Shooting method	DTM-Padé	Shooting method
0.1	−1.265 492 575 299 778	−1.265 492 575 299 777 9	−0.853 300 068 364 298 8	−0.853 300 068 364 298 8
0.2	−1.265 274 871 787 588	−1.265 274 871 787 588 8	−0.854 905 242 597 022 7	−0.854 905 242 597 022 6

Figure 2 represents the effects of the squeeze Reynolds number and magnetic force strength in the axial direction on the axial velocity f'. The results show that when the values of R_{Q} and R_{M} increase, the axial velocity decreases significantly. Further, the tangential velocity increases when the magnetic force strength increases while decreases when the squeeze Reynolds number increases (see Fig. 3). Figure 4 shows the effects of the magnetic Reynolds number M_{R} on the axial and tangential induced magnetic fields. From this figure, it is keenly observed that when the values of M_{R} increase, the axial and tangential induced magnetic fields significantly decrease.

Figure 5 displays the effects of the thermophoresis parameter T_{t} and Brownian motion parameter T_{b} with fixed values of other parameters on the temperature. The results reveal that when the thermophoresis parameter increases, the temperature increases. A similar phenomenon is also noticed against the Brownian motion parameter for the temperature. The effects of the Prandtl number Pr and squeeze Reynolds number R_{Q} on the dimensionless temperature can be seen in Fig. 6. It is understood that for superior values of the Prandtl number Pr, the temperature decreases over the whole region λ, because increasing the Prandtl number enhances the momentum diffusivity, which results in the decrease in the temperature. It is also perceived that the temperature significantly falls with the increase in the squeeze Reynolds number R_{Q}.

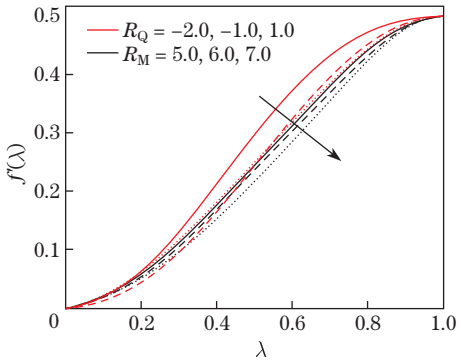

Fig. 2 Effect of different values of the squeeze Reynolds number R_Q, magnetic force strength R_M on the axial velocity distribution $f'(\lambda)$ (color online)

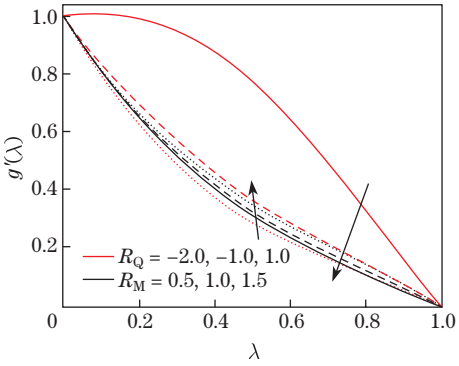

Fig. 3 Effects of different values of the squeeze Reynolds number R_Q and magnetic force strength R_M on the tangential velocity $g'(\lambda)$ (color online)

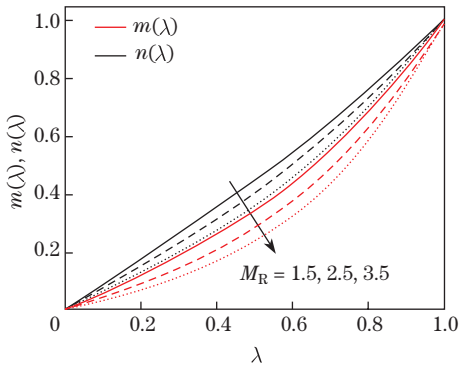

Fig. 4 Effects of different values of the magnetic Reynolds number M_R on the axial and tangential induced magnetic fields $m(\lambda)$ and $n(\lambda)$ (color online)

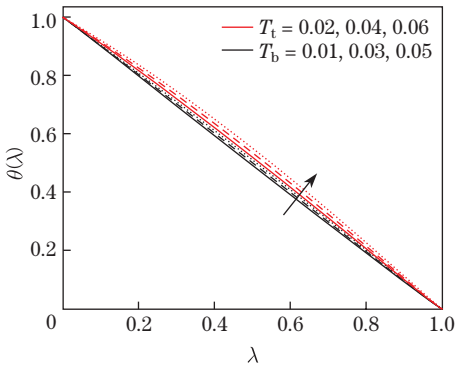

Fig. 5 Effects of different values of the thermophoresis parameter T_t and Brownian motion parameter T_b on the temperature $\theta(\lambda)$ (color online)

The effects of the thermophoresis parameter T_t and Brownian motion parameter T_b on the nanoparticle concentration are shown in Fig. 7. It reveals that the nanoparticle concentration decreases when the values of T_b increase. Moreover, quite similar phenomena occur while the values of T_t increase. The effects of the squeeze Reynolds number R_Q and magnetic Reynolds number M_R on the nanoparticle concentration field ϕ are shown in Fig. 8. It can be seen that the nanoparticle concentration increases with the increase in the values of the squeeze Reynolds number while decreases with the increase in the Schmidt number Sc.

The effects of the squeeze Reynolds number R_Q and Peclet number Pe on the microorganism density χ are sketched in Fig. 9. It is perceived that the microorganism density χ increases when the values of the squeeze Reynolds number R_Q increase while decreases when the values of the Peclet number Pe increase.

Therefore, when the values of Pe increase, the speed and diffusivity of the microorganisms decrease. Figure 10 is displayed to get the physical behaviors of the Schmidt number Sc. It is shown that when the values of the Schmidt number Sc increase, the microorganism density increases, but the effects are minimal.

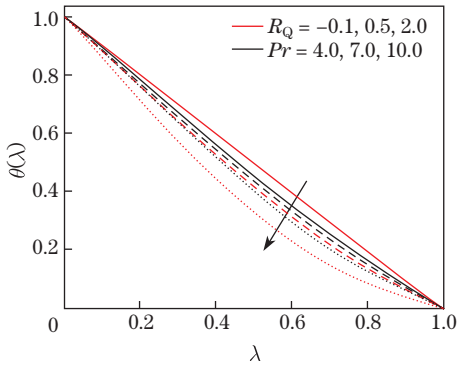

Fig. 6 Effects of different values of the squeeze Reynolds number R_Q and Prandtl number Pr on the temperature $\theta(\lambda)$ (color online)

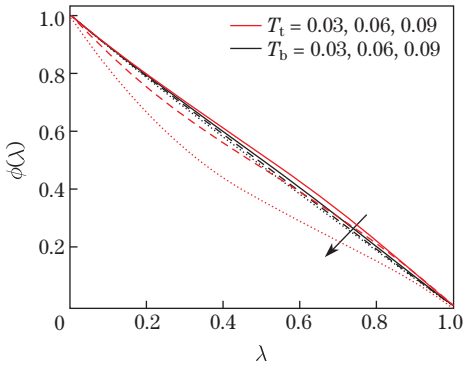

Fig. 7 Effects of different values of the thermophoresis parameter T_t and Brownian motion parameter T_b on the nanoparticle concentration $\phi(\lambda)$ (color online)

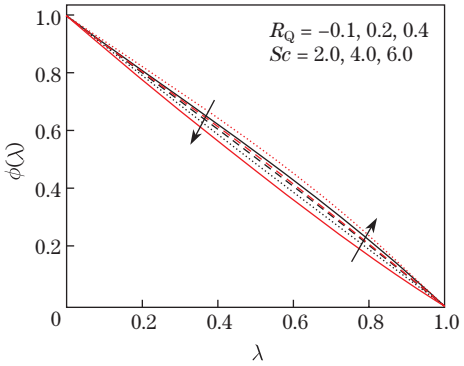

Fig. 8 Effects of different values of the squeeze Reynolds number R_Q and Schmidt number Sc on the nanoparticle concentration $\phi(\lambda)$ (color online)

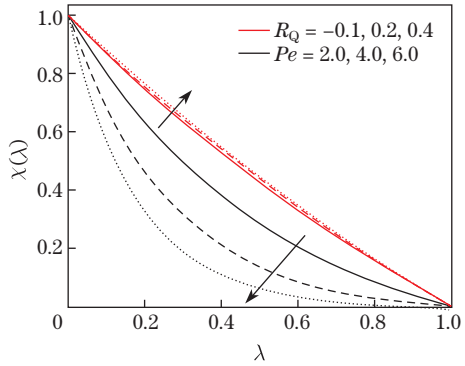

Fig. 9 Effects of different values of the squeeze Reynolds number R_Q and Peclet number Pe on the motile microorganism density $\chi(\lambda)$ (color online)

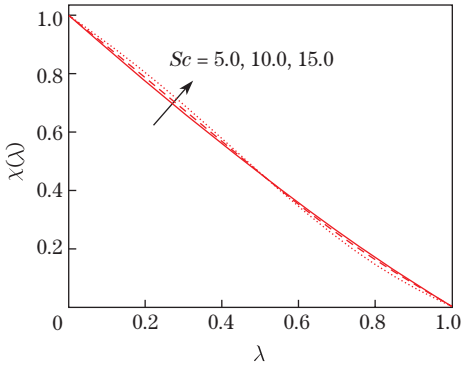

Fig. 10 Effects of different values of the Schmidt number Sc on the motile microorganism density $\chi(\lambda)$ (color online)

5 Conclusions

In this article, the three-dimensional (3D) flow between a pair of rotating circular plates in the existence of an induced magnetic field is investigated. The fluid comprises the nanoparticles and gyrotactic microorganisms. The mathematical modeling is formulated with the help of 3D similarity transformations. The DTM is used to solve the resulting differential equations. However, the convergence rate is slow, and boundary conditions are not satisfied at $\lambda = 1$. Therefore, the Padé approximation is merged with the DTM to obtain the required convergence. It is seen that after combining the DTM with the Padé approximation, the results are quite similar to the numerical shooting method. The results show that the DTM-Padé method is a powerful technique compared with any other similar method[38]. Here, we get a convergence up to order $[5 \times 5]$. The DTM-Padé method is accurate and stable. It has a broad applicability in many problems such as chemo-thermo-fluid dynamics. An excellent correlation of the DTM-Padé technique with the shooting method is carried out. The main findings are summarized as follows:

(I) The magnetic force strength shows converse behaviors for the axial and tangential velocities.

(II) The squeeze Reynolds number significantly suppresses the axial and tangential velocities.

(III) The magnetic Reynolds number tends to diminish the induced magnetic field in the axial and tangential directions.

(IV) The Brownian motion reveals opposite effects on the temperature and nanoparticle concentration while similar effects on the thermophoresis properties.

(V) The squeeze Reynolds number significantly suppresses the temperature, microorganism, and nanoparticle concentration.

(VI) The Peclet number tends to diminish the microorganism density, whereas the Schmidt number tends to boost the microorganism density.

References

[1] EASTMAN, J. A. and CHOI, S. U. S. Enhancing thermal conductivity of fluids with nanoparticles. *ASME International Mechanical Engineering Congress and Exposition*, San Fransisco, 99–105 (1995)

[2] Pak, B. C. and CHO, Y. I. Hydrodynamic and heat transfer study of dispersed fluids with submicron metallic oxide particles. *Experimental Heat Transfer: An International Journal*, **11**, 151–170 (1998)

[3] LIN, J. Z. and YANG, H. L. A review on the flow instability of nanofluids. *Applied Mathematics and Mechanics* (*English Edition*), **40**(9), 1227–1238 (2019) https://doi.org/10.1007/s10483-019-2521-9

[4] DAS, S. K., PUTRA, N., THIESEN, P., and ROETZEL, W. Temperature dependence of thermal conductivity enhancement for nanofluids. *Journal of Heat Transfer*, **125**, 567–574 (2003)

[5] XUAN, Y. and ROETZEL, W. Conceptions for heat transfer correlation of nanofluids. *International Journal of Heat and Mass Transfer*, **43**, 3701–3707 (2000)

[6] GHERASIM, I., ROY, G., NGUYEN, C. T., and VO-NGOC, D. Experimental investigation of nanofluids in confined laminar radial flows. *International Journal of Thermal Sciences*, **48**, 1486–1493 (2009)

[7] ZHANG, X., GU, H., and FUJII, M. Effective thermal conductivity and thermal diffusivity of nanofluids containing spherical and cylindrical nanoparticles. *Experimental Thermal and Fluid Science*, **31**, 593–599 (2007)

[8] HAMILTON, R. L. and CROSSER, O. K. Thermal conductivity of heterogeneous two-component systems. *Industrial and Engineering Chemistry Fundamentals*, **1**, 187–191 (1962)

[9] SHEIKHOLESLAMI, M., HAYAT, T., and ALSAEDI, A. MHD free convection of Al_2O_3-water nanofluid considering thermal radiation: a numerical study. *International Journal of Heat and Mass Transfer*, **96**, 513–524 (2016)

[10] FAKOUR, M., VAHABZADEH, A., and GANJI, D. D. Study of heat transfer and flow of nanofluid in permeable channel in the presence of magnetic field. *Propulsion and Power Research*, **4**, 50–62 (2015)

[11] ELLAHI, R., ZEESHAN, A., HUSSAIN, F., and ABBAS, T. Thermally charged MHD bi-phase flow coatings with non-Newtonian nanofluid and hafnium particles along slippery walls. *Coatings*, **9**, 300 (2019)

[12] ZHU, J., WANG, S., ZHENG, L., and ZHANG, X. Heat transfer of nanofluids considering nanoparticle migration and second-order slip velocity. *Applied Mathematics and Mechanics* (*English Edition*), **38**(1), 125–136 (2017) https://doi.org/10.1007/s10483-017-2155-6

[13] BASKAYA, E., KOMURGOZ, G., and OZKOL, I. Investigation of oriented magnetic field effects on entropy generation in an inclined channel filled with ferrofluids. *Entropy*, **19**, 377 (2017)

[14] HAMID, M., USMAN, M., HAQ, R. U., KHAN, Z. H., and WANG, W. Wavelet analysis of stagnation point flow of non-Newtonian nanofluid. *Applied Mathematics and Mechanics* (*English Edition*), **40**(8), 1211–1226 (2019) https://doi.org/10.1007/s10483-019-2508-6

[15] ZEESHAN, A., SHEHZAD, N., ABBAS, T., and ELLAHI, R. Effects of radiative electromagnetohydrodynamics diminishing internal energy of pressure-driven flow of titanium dioxide-water nanofluid due to entropy generation. *Entropy*, **21**, 236 (2019)

[16] IMTIAZ, M., SHAHID, F., HAYAT, T., and ALSAEDI, A. Melting heat transfer in Cu-water and Ag-water nanofluids flow with homogeneous-heterogeneous reactions. *Applied Mathematics and Mechanics* (*English Edition*), **40**(4), 465–480 (2019) https://doi.org/10.1007/s10483-019-2462-8

[17] HUSSAIN, F., ELLAHI, R., ZEESHAN, A., and VAFAI, K. Modelling study on heated couple stress fluid peristaltically conveying gold nanoparticles through coaxial tubes: a remedy for gland tumors and arthritis. *Journal of Molecular Liquids*, **268**, 149–155 (2018)

[18] ELLAHI, R., HASSAN, M., and ZEESHAN, A. Shape effects of nanosize particles in Cu-H_2O nanofluid on entropy generation. *International Journal of Heat and Mass Transfer*, **81**, 449–456 (2015)

[19] HEIDARY, H., HOSSEINI, R., PIRMOHAMMADI, M., and KERMANI, M. J. Numerical study of magnetic field effect on nano-fluid forced convection in a channel. *Journal of Magnetism and Magnetic Materials*, **374**, 11–17 (2015)

[20] LIN, J., XIA, Y., and KU, X. K. Friction factor and heat transfer of nanofluids containing cylindrical nanoparticles in laminar pipe flow. *Journal of Applied Physics*, **116**, 133513 (2014)

[21] LIN, J. Z., XIA, Y., and KU, X. K. Pressure drop and heat transfer of nanofluid in turbulent pipe flow considering particle coagulation and breakage. *Journal of Heat Transfer*, **136**, 111701 (2014)

[22] LIN, J. Z., XIA, Y., and KU, X. K. Flow and heat transfer characteristics of nanofluids containing rod-like particles in a turbulent pipe flow. *International Journal of Heat and Mass Transfer*, **93**, 57–66 (2016)

[23] SOBAMOWO, M. G., JAYESIMI, L. O., and WAHEED, M. A. Magnetohydrodynamic squeezing flow analysis of nanofluid under the effect of slip boundary conditions using variation of parameter method. *Karbala International Journal of Modern Science*, **4**, 107–118 (2018)

[24] VAJRAVELU, K., PRASAD, K. V., NG, C. O., and VAIDYA, H. MHD squeeze flow and heat transfer of a nanofluid between parallel disks with variable fluid properties and transpiration. *International Journal of Mechanical and Materials Engineering*, **12**, 9 (2017)

[25] HOSSEINZADEH, K., ALIZADEH, M., and GANJI, D. D. Hydrothermal analysis on MHD squeezing nanofluid flow in parallel plates by analytical method. *International Journal of Mechanical and Materials Engineering*, **13**, 4 (2018)

[26] HASHMI, M. M., HAYAT, T., and ALSAEDI, A. On the analytic solutions for squeezing flow of nanofluid between parallel disks. *Nonlinear Analysis*: *Modelling and Control*, **17**, 418–430 (2012)

[27] SINGH, K., RAWAT, S. K., and KUMAR, M. Heat and mass transfer on squeezing unsteady MHD nanofluid flow between parallel plates with slip velocity effect. *Journal of Nanoscience*, 1–11 (2016)

[28] BHATTA, D. P., MISHRA, S. R., and DASH, J. K. Unsteady squeezing flow of water-based nanofluid between two parallel disks with slip effects: analytical approach. *Heat Transfer–Asian Research*, **48**, 1–20 (2019)

[29] MADAKI, A. G., ROSLAN, R., MOHAMED, M., and KAMARDAN, M. G. Analytical solutions of squeezing unsteady nanofluid flow in the presence of thermal radiation. *Journal of Computer Science and Computational Mathematics*, **6**, 451–463 (2016)

[30] VIMALA, P. and MANIMEGALAI, K. Natural convection flow of nanofluids in squeeze film with an exponential curvature. *Journal of Informatics and Mathematical Sciences*, **10**, 371–381 (2010)

[31] ACHARYA, N., DAS, K., and KUNDU, P. K. The squeezing flow of Cu-water and Cu-kerosene nanofluids between two parallel plates. *Alexandria Engineering Journal*, **55**, 1177–1186 (2016)

[32] THONGMOON, M. and PUSJUSO, S. The numerical solutions of differential transform method and the Laplace transform method for a system of differential equations. *Nonlinear Analysis*: *Hybrid Systems*, **4**, 425–431 (2010)

[33] FATOOREHCHI, H. and ABOLGHASEMI, H. Differential transform method to investigate mass transfer phenomenon to a falling liquid film system. *Australian Journal of Basic and Applied Sciences*, **5**, 337–345 (2011)

[34] YOUSIF, M. A., HATAMI, M., and ISMAEL, H. F. Heat transfer analysis of MHD three dimensional Casson fluid flow over a porous stretching sheet by DTM-Padé. *International Journal of Applied and Computational Mathematics*, **3**, 813–828 (2017)

[35] ÇILINGIR, S., İNCI, A. A., BULUT, H., HAMMOUCH, Z., BASKONUS, H. M., MEKKAOUI, T., MUHAMMAD, B., and BIN, F. Numerical investigation on MHD flow and heat transfer over an exponentially stretching sheet with viscous dissipation and radiation effects, *ITM Web of Conferences*, **13**, 01025 (2017)

[36] KHAN, W. A., RASHAD, A. M., ABDOU, M. M. M., and TLILI, I. Natural bioconvection flow of a nanofluid containing gyrotactic microorganisms about a truncated cone. *European Journal of Mechanics-B/Fluids*, **75**, 133–142 (2019)

[37] SALEEM, S., RAFIQ, H., AL-QAHTANI, A., EL-AZIZ, M. A., MALIK, M. Y., and ANIMASAUN, I. L. Magneto Jeffrey nanofluid bioconvection over a rotating vertical cone due to gyrotactic microorganism. *Mathematical Problems in Engineering*, **2019**, 3478037 (2019)

[38] KHAN, W. A., MAKINDE, O. D., and KHAN, Z. H. MHD boundary layer flow of a nanofluid containing gyrotactic microorganisms past a vertical plate with Navier slip. *International Journal of Heat and Mass Transfer*, **74**, 285–291 (2014)

[39] FAROOQ, S., HAYAT, T., ALSAEDI, A., and AHMAD, B. Numerically framing the features of second order velocity slip in mixed convective flow of Sisko nanomaterial considering gyrotactic microorganisms. *International Journal of Heat and Mass Transfer*, **112**, 521–532 (2017)

[40] WAQAS, H., KHAN, S. U., HASSAN, M., BHATTI, M. M., and IMRAN, M. Analysis on the bioconvection flow of modified second-grade nanofluid containing gyrotactic microorganisms and nanoparticles. *Journal of Molecular Liquids*, **291**, 111231 (2019)

[41] WAQAS, H., KHAN, S. U., IMRAN, M., and BHATTI, M. M. Thermally developed Falkner-Skan bioconvection flow of a magnetized nanofluid in the presence of a motile gyrotactic microorganism: Buongiorno's nanofluid model. *Physica Scripta*, **94**, 115304 (2019)

[42] AZIZ, A., KHAN, W. A., and POP, I. Free convection boundary layer flow past a horizontal flat plate embedded in porous medium filled by nanofluid containing gyrotactic microorganisms. *International Journal of Thermal Sciences*, **56**, 48–57 (2012)

[43] RAEES, A., XU, H., SUN, Q., and POP, I. Mixed convection in gravity-driven nano-liquid film containing both nanoparticles and gyrotactic microorganisms. *Applied Mathematics and Mechanics* (*English Edition*), **36**(2), 163–178 (2015) https://doi.org/10.1007/s10483-015-1901-7

[44] MEADE, D. B., HARAN, B. S., and WHITE, R. E. The shooting technique for the solution of two-point boundary value problems. *Maple Technical Newsletter*, **3**, 1–8 (1996)